ACS APPLIED MATERIALS & INTERFACES

Research Article

www.acsami.org

Cross-Linked Gold Nanoparticles on Polyethylene: Resistive Responses to Tensile Strain and Vapors

Natalia Olichwer, Elisabeth W. Leib, Annelie H. Halfar,† Alexey Petrov, and Tobias Vossmeyer*

Institute of Physical Chemistry, University of Hamburg, Grindelallee 117, 20146 Hamburg, Germany

Supporting Information

ABSTRACT: In this study, coatings of cross-linked gold nanoparticles (AuNPs) on flexible polyethylene (PE) substrates were prepared via layer-by-layer deposition and their application as strain gauges and chemiresistors was investigated. Special emphasis was placed on characterizing the influence of strain on the chemiresistive responses. The coatings were deposited using amine stabilized AuNPs (4 and 9 nm diameter) and 1,9-nonanedithiol (NDT) or pentaerythritol tetrakis(3-mercaptopropionate) (PTM) as cross-linkers. To prepare films with homogeneous optical appearance, it was necessary to treat the substrates with oxygen plasma directly before film assembly. SEM images revealed film thicknesses between ~60 and ~90 nm and a porous nanoscale morphology. All films showed ohmic I-V characteristics with conductivities ranging from 1×10^{-4} to 1×10^{-2} Ω^{-1} cm^{-1}, depending on the structure of the linker and the nanoparticle size. When up to 3% strain was induced their resistance increased linearly and reversibly (gauge factors: ~20). A comparative SEM investigation indicated that the stress induced formation and extension of nanocracks are important components of the signal transduction mechanism. Further, all films responded with a reversible increase in resistance when dosed with toluene, 4-methyl-2-pentanone, 1-propanol or water vapor (concentrations: 50−10 000 ppm). Films deposited onto high density PE substrates showed much faster response-recovery dynamics than films deposited onto low density PE. The chemical selectivity of the coatings was controlled by the chemical nature of the cross-linkers, with the highest sensitivities (~1×10^{-5} ppm^{-1}) measured with analytes of matching solubility. The response isotherms of all film/vapor pairs could be fitted using a Langmuir−Henry model suggesting selective and bulk sorption. Under tensile stress (1% strain) all chemiresistors showed a reversible increase in their response amplitudes (~30%), regardless of the analytes' permittivity. Taking into consideration the thermally activated tunneling model for charge transport, this behavior was assigned to stress induced formation of nanocracks, which enhance the films' ability to swell in lateral direction during analyte sorption.

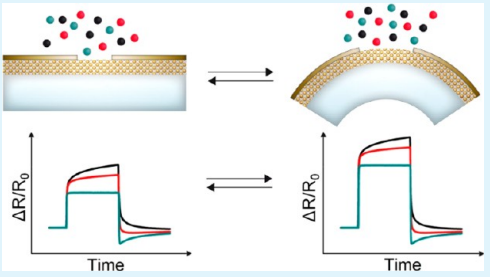

KEYWORDS: *gold, nanoparticle, film, coating, polyethylene, chemiresistor, strain gauge*

INTRODUCTION

The conductivity σ of thin films composed of ligand-stabilized gold nanoparticles (AuNPs) is commonly described by thermally activated tunneling of charge carriers. A widely used mathematical representation of this model is given by the following equation[1]

$$\sigma = \sigma_0 e^{-\beta\delta} e^{-E_a/RT} \quad (1)$$

Here, $\sigma_0 \exp(-\beta\delta)$ is the conductivity at infinite temperature, β is the tunneling decay constant, and δ is the surface-to-surface distance between neighboring metal cores, i.e. the tunneling distance. The Arrhenius term takes into account thermal activation of charge carriers. Attempts have been made to attribute the activation energy E_a to the Coulomb charging energy of the particles or to the reorganizational energy according to Marcus theory.[1,2] Importantly, in both models E_a is inversely proportional to the relative permittivity of the nanoparticles' environment and increases with increasing interparticle distance.

Because of its exponential dependence on E_a and δ, the conductivity of these films is highly sensitive to any perturbation of these parameters. Thus, applications of films fabricated from ligand-stabilized AuNPs as resistive sensing elements have been studied intensively[3−11] and pushed toward specific applications in several laboratories.[12−16] For discussing the response characteristics of these sensors it is convenient to rearrange eq 1 into the following form[9,17]

$$\frac{\Delta R}{R_0} = e^{\beta\Delta\delta} e^{\Delta E_a/RT} - 1 \quad (2)$$

Here, R_0 is the baseline resistance and ΔR, $\Delta\delta$, ΔE_a are the changes in resistance, interparticle distance, and activation energy, which could, for example, be caused by sorption of an analyte or stress.

Chemiresistors based on films of metal nanoparticles usually respond with an increase in resistance to analyte sorption. This effect has been attributed to swelling of the films, leading to increased tunneling distances.[3,9] On the other hand, it has also been shown that rigidly cross-linked nanoparticle films, which have only very limited freedom to swell, respond with a

Received: August 24, 2012
Accepted: November 5, 2012
Published: November 5, 2012

 © 2012 American Chemical Society dx.doi.org/10.1021/am301780b | ACS Appl. Mater. Interfaces 2012, 4, 6151−6161

decrease in resistance to analyte sorption.[18] This effect has been attributed to a decrease in the activation energy, caused by the increase in permittivity due to sorption of the analyte within voids. Taken together, the net responses of chemiresistors based on ligand-stabilized metal nanoparticles is the result of two counteracting effects: Swelling causes an increase in resistance due to increased tunneling distances, whereas void-filling - or displacement of ligands by analytes of higher permittivity - decreases the resistance by augmenting the effective permittivity in the nanoparticles' environment. In fact, several experimental studies confirm this interpretation.[9,19,20] However, results reported by Lewis and co-workers[21] suggest that a more quantitative description of the sensing mechanism requires a deeper understanding of the structural rearrangements induced by vapor sorption. The most important achievements of investigations into the sensing mechanism and new trends for applications of these chemiresistors have recently been summarized in a comprehensive review by Ibañez and Zamborini.[22]

Another interesting application which uses the dependence of the resistance on changes in interparticle distances are strain gauges. Herrmann et al.[10] produced strain gauges by depositing AuNPs on inkjet transparencies and reported sensitivities 2 orders of magnitude higher than that of conventional metal foil gauges. Similar results were obtained by us[11] and by Farcau et al.[23,24] who investigated strain gauges fabricated from wire-patterned monolayers and multilayers of AuNPs. Kulkarni and co-workers[25] reported gauge factors up to 390 for strain sensors based on micromolded Pd-nanoparticle-carbon μ-stripes.

While the studies referenced above focused either on the application of AuNP-films as chemical sensors or strain sensors, one pioneering study by Zhong and co-workers[26] investigated the concerted influence of both strain and vapor sorption on the resistivity of these films. Interestingly, this study showed that the surrounding vapor atmosphere can significantly affect the strain gauge responses. The quite complex data sets presented were interpreted qualitatively by taking into account analyte partitioning and the analyte's permittivity. Clearly, the rational development of sensors based on flexible AuNP-coatings, which are robust against unwanted signal interferences when operated under harsh conditions, as well as the design of novel dual chemical/strain sensors, requires further research efforts. In addition, the possibility to induce structural changes within the sensitive coatings by straining the substrates provides highly interesting opportunities to study structure/sensitivity relationships and to improve our current understanding of the underlying sensing mechanisms.

In our previous contribution,[11] we reported on the preparation and the charge transport properties of non-anedithiol (NDT) cross-linked AuNP-coatings deposited onto low density polyethylene (LDPE) substrates. It was demonstrated that these coatings are mechanically robust and very well suited for strain gauge applications. Motivated by this result we have now significantly extended our investigations: First, we investigated if polyethylene (PE) substrates allow for the application of cross-linked AuNP-coatings as flexible chemiresistors. As shown here, high density polyethylene (HDPE) provides an excellent substrate for this purpose, whereas LDPE has some drawbacks due to its higher vapor permeability. Second, we varied the composition of the films in order to test the influence of different particle sizes and different linker structures on both, the strain gauge and chemiresistive responses. Surprisingly, the variation in particle size had only little influence on the strain gauge properties. However, the chemical selectivity of the films clearly changed toward more polar analytes when using a more polar cross-linker. Third, and most importantly, we investigated the influence of strain on the chemiresistive responses. We show that the sensitivity of the films was significantly enhanced when the films were under strain, regardless of the analytes's permittivity. Supported by a comparative SEM study, we attribute this effect to strain induced formation of nanoscale cracks, which enhances the ability of the film to swell during vapor sorption.

EXPERIMENTAL SECTION

Materials. Chemicals were purchased from Aldrich, Fluka, Th. Geyer GmbH & Co. KG and Grüssing GmbH. All chemicals and solvents except oleylamine (70 wt %) were of analytical grade and used as received. Deionized water (resistivity: 18.2 MΩ cm) was purified using a Millipore Simplicity system. Polyethylene substrates with a diameter of 40 mm and a thickness of 0.56 mm were prepared by injection molding (HAAKE MiniJet system) using low-density polyethylene (LDPE, Aldrich) with a melt index of 25 g/10 min (190 °C/2.16 kg) and high-density polyethylene (HDPE, Aldrich) with a melt index of 42 g/10 min (190 °C/2.16 kg). Dodecylamine-stabilized AuNPs with an average diameter of 4 nm were synthesized as described previously.[8,27] Oleylamine-stabilized AuNPs with a core size of 9 nm were synthesized following the method of Shen et al.[28] and using a reaction temperature of 95 °C. After purification via fractionated precipitation with ethanol used as nonsolvent, the AuNPs were dissolved in toluene and stored in a refrigerator. TEM images and size-histograms of AuNPs used in this study are provided as Supporting Information (Figure S1).

Film Preparation. AuNP-films were prepared via the layer-by-layer self-assembly method.[8,29] Prior to film deposition, the polyethylene substrates were treated with oxygen plasma (Plasma Prep II, SPI Supplies) for 20 min. The oxygen pressure was 0.67 mbar and the current 40 mA. Immediately after the plasma treatment, the oxidized substrates were immersed into the solution of AuNPs in toluene with the concentration adjusted to an absorbance of 1.2 at the plasmon absorption maximum, at 1 cm path length. Taking into account the cubic scaling of the extinction coefficient of AuNPs with particle size, the particle concentration of the solution containing the larger oleylamine-stabilized AuNPs was approximately 1 order of magnitude lower than that of the smaller dodecylamine-stabilized AuNPs. After 5 min the substrates were washed with toluene and then immersed into a solution of the linker in toluene (6 mmol/L) for 5 min. As the last step of one deposition cycle the substrates were washed again with toluene. The film preparation was completed after finishing 22 deposition cycles. We note that shortening the time of plasma treatment to 30 s and reducing the current to 35 mA had only little influence on the visual appearance of prepared AuNP-coatings (see the Supporting Information, Table S1). In order to deposit the oleylamine-stabilized AuNPs, we first had to deposit dodecylamine-stabilized AuNPs as an adhesion layer (three deposition cycles). The oleylamine-stabilized AuNPs were then deposited as explained above (19 deposition cycles). After completing the assembly process the films were dried in ambient air and then stored under nitrogen until needed.

ATR-FTIR Spectroscopy. IR spectra of the substrate surfaces were recorded using a Bruker Equinox 55 spectrometer equipped with a diamond crystal as ATR-IR element.

Resistance Measurements. Gold electrode pairs of nominal 100 nm thickness and 400 μm spacing were deposited onto the gold nanoparticle films by vacuum evaporation (Pfeiffer, Classic 250) through a shadow mask. To measure strain induced resistance changes the devices were placed into sample holders made of acrylic glass allowing for defined convex bending of the substrates.[11] The tensile strain, determined by the substrate thickness and the radius of curvature of the holders, was 0.25, 0.5, 1, 1.5, 2, 2.5, and 3%. For the

resistance measurements, a Keithley multimeter 2000 was employed. The $I-V$ curves were recorded using a Keithley sourcemeter 2601A. Unless otherwise indicated, the measurements were carried out at ambient conditions (~298 K, ~50% relative humidity).

Electron Microscopy. TEM images of AuNPs were measured with a JEOL 1011, 100 kV, LaB_6 microscope. To stabilize the 4 nm AuNPs for TEM investigations the dodecylamine ligands were exchanged by dodecanethiol, as described previously.[30] SEM images of the films were recorded using a LEO-1550 (Carl Zeiss) field-emission scanning electron microscope.

To examine possible changes in the film morphology caused by tensile strain, we measured selected areas of the film $Au_{4\ nm}$NDT first under no strain and then under 3% tensile strain. For these measurements a rather low acceleration voltage of 1 kV was used in order to avoid any deformation of the sample due to energy input. The images were taken with 25 000-fold magnification. Increasing the magnification led to blurred images and carbon contaminations making it difficult to observe the subtle structural changes induced by strain. To better recognize subtle structural differences, we used the backscatter detector to enhance the Z-contrast.

For imaging cross-sections of the films, the sensors were frozen in liquid nitrogen and then cleaved.

Vapor Sensing Measurements. Test vapors were generated using a commercial programmable calibration system (Kalibriersystem Model CGM 2000, Umwelttechnik MCZ). As carrier gas nitrogen 5.0 was used. The flow through the sensor test chamber (glass, ~40 mL) was adjusted to a rate of 400 mL/min. The samples were placed into holders (Teflon) which allowed for controlled bending. According to the curvature of these holders it was possible to induce a strain of −1, 0, 1, 2, and 3% in the sensor films. Unless otherwise indicated, the chemiresistor signals were acquired by supplying a constant current of 100 nA (Keithley Sourcemeter 2601A) and measuring the change in voltage (Keithley Multimeter 2002). All experiments were carried out at room temperature.

RESULTS AND DISCUSSION

Deposition of Cross-Linked AuNP Films onto Polyethylene Substrates and Their Morphology. Our method for depositing cross-linked AuNPs onto high density polyethylene (HDPE) substrates is based on layer-by-layer self-assembly.[11,29] Before depositing the first layer of AuNPs, we cleaned the substrates and functionalized them by exposing them to oxygen-plasma. As reported by several authors,[31−34] the exposure of polyethylene to oxygen plasma leads to the formation of functional groups (e.g., −OH, −CHO, −COOH) and at the same time to the deterioration of hydrocarbon chains. After the plasma treatment, we observed an increase in the wettability of the substrates by water. The advancing contact angle decreased from ~83° to ~39°. This observation indicates the formation of polar surface groups. Attenuated total reflectance Fourier transform infrared (ATR-FTIR) spectroscopy performed before and after plasma treatment revealed the decomposition of some functional surface groups (see the Supporting Information, Figure S2), which we attribute to surface contaminants and/or the presence of a slip agent.[35] It was, however, impossible to detect the formation of new oxidized carbon species, showing that the surface density of polar groups generated by plasma treatment was rather low. Directly after plasma treatment the AuNP-films were deposited onto the substrates.

Comparative experiments revealed that omitting the plasma treatment resulted in the formation of rather inhomogeneous and thinner AuNP coatings (see the Supporting Information, Table S1). Thus, plasma etching of the substrate was indeed necessary to deposit homogeneously appearing coatings. Plasma-generated polar surface groups probably accelerate the deposition process. Carboxylate groups, for example, have some affinity to gold nanoparticles as known from citrate-stabilized AuNPs. Also, spontaneous self-assembly of nanoparticles at polar/nonpolar interfaces has been reported by Lin et al.,[36] previously.

In our present study, we prepared three different film materials, two of them, $Au_{4\ nm}$NDT and $Au_{4\ nm}$PTM, both consisted of 4 nm sized AuNPs, but different cross-linkers. The structures of the cross-linkers, 1,9-nonanedithiol (NDT) and pentaerythritol tetrakis(3-mercaptopropionate) (PTM), are shown in Scheme 1.

Scheme 1. Gold Nanoparticle Film Based Resistor Equipped with Gold Electrodes (typical dimensions); Zoom: Cross-Linked Gold Nanoparticles Swollen with Solvent; NDT and PTM were Used As Linker Molecules

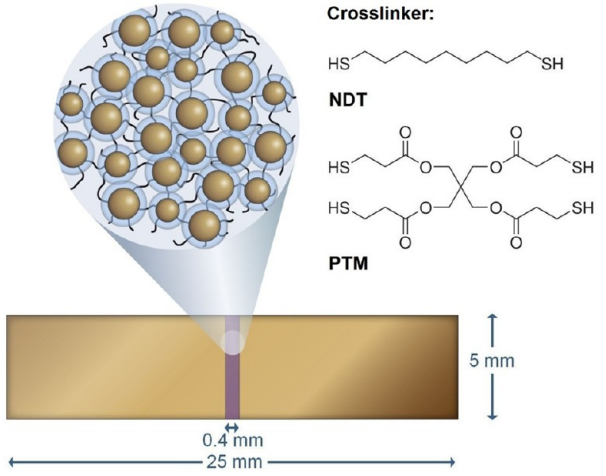

NDT is a simple, hydrophobic alkanedithiol. In contrast, PTM comprises four polar ester groups, capable of acting as hydrogen-bond acceptors, and four thiol groups for cross-linking AuNPs. Both compounds are commercially available and were chosen to study the influence of the linker polarity on the chemical selectivity of the films. As the nanoparticle component, we used dodecylamine-stabilized AuNPs. During film assembly, the amine ligands are quickly replaced by thiolated cross-linkers.[8] On the macroscopic scale both films, $Au_{4\ nm}$NDT and $Au_{4\ nm}$PTM, had a homogeneous optical appearance with a purple-bluish color in transmission and metallic-like reflection (see the Supporting Information, Figure S3). The SEM images presented in Figure 1a−d reveal quite continuous coatings on the micrometer scale. On the submicrometer scale, however, the $Au_{4\ nm}$NDT-film showed cracks with lengths up to ~300 nm and widths up to ~50 nm. In striking contrast the $Au_{4\ nm}$PTM-film showed a porous morphology, with pore diameters up to ~50 nm.

The approximate thicknesses of these coatings were determined from profile SEM images (see the Supporting Information, Figure S4) and are presented in Table 1.

To investigate any possible influence of the particle size on the sensing properties we prepared a third film, $Au_{9\ nm}$NDT using oleylamine-stabilized AuNPs with a core diameter of 9 nm and NDT as cross-linker. Attempts to deposit these particles directly onto plasma-treated PE-substrates failed in that the assembly process was significantly slowed down. We explain this observation by the longer chain length of the oleylamine ligands, which provides the particles with more

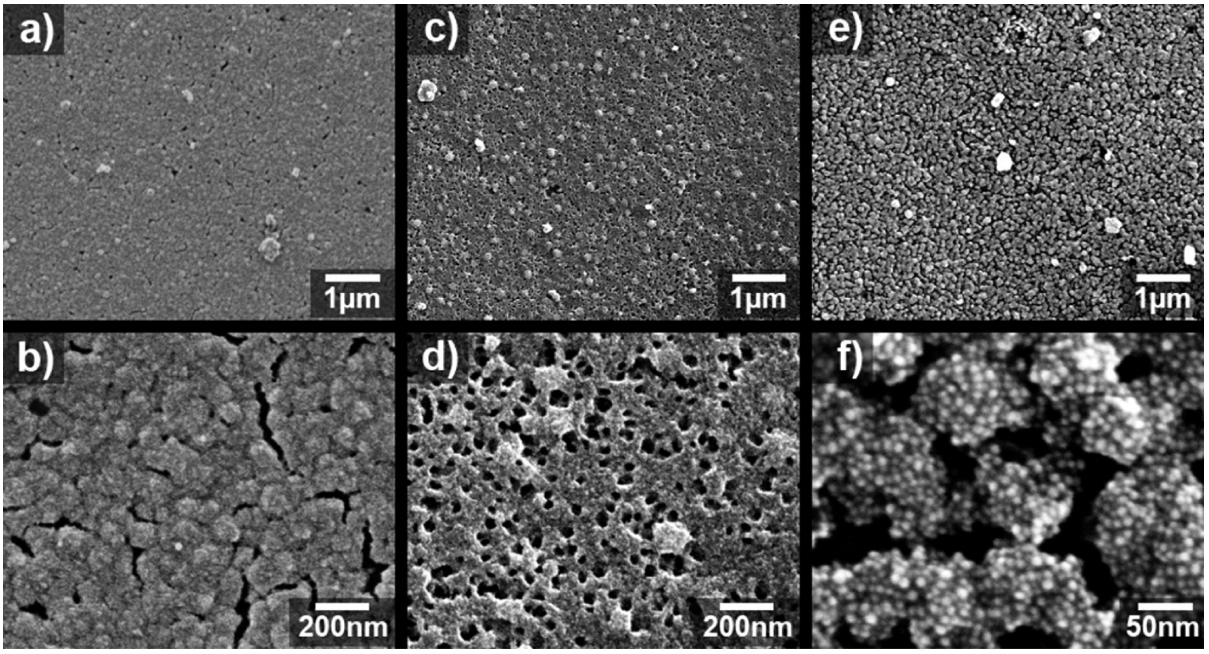

Figure 1. SEM images in two different magnifications of the films (a, b) $Au_{4\ nm}$NDT, (c, d) $Au_{4\ nm}$PTM, (e, f) $Au_{9\ nm}$NDT.

Table 1. Characteristics of AuNP Films Deposited onto HDPE

	$Au_{4\ nm}$NDT	$Au_{4\ nm}$PTM	$Au_{9\ nm}$NDT
sheet resistance (MΩ)	18.5 ± 3.3	352 ± 84	10.7 ± 1.9
thickness (nm)[a]	~90	~70	~60
conductivity ($\Omega^{-1}cm^{-1}$)[b]	$6 \times 10^{-3} \pm 1 \times 10^{-3}$	$4 \times 10^{-4} \pm 1 \times 10^{-4}$	$2 \times 10^{-2} \pm <1 \times 10^{-2}$
gauge factor[c]	21 (21)	18 (16)	24 (32)

[a]The thickness was estimated from the SEM images of the breaking edge (Figure S4, Supporting Information). [b]The standard deviations were calculated from 3 to 6 measured values. [c]Gauge factors in parentheses were measured under nitrogen atmosphere.

efficient sterical stabilization. In order to accelerate the deposition of oleylamine-stabilized AuNPs we first deposited a thin adhesion layer using the less stable dodecylamine-stabilized AuNPs (3 deposition cycles). After this layer was functionalized with thiol groups of the NDT linker, the oleylamine-stabilized AuNPs could be deposited within reasonable reaction times (5 min per deposition step). Compared to films prepared with the smaller AuNPs, SEM images e and f in Figure 1 reveal a less continuous coating with granular structures consisting of clustered nanoparticles. A statistical analysis of several SEM images showed that ~75% of the substrate surface was covered by the film. As determined by SEM profile images (see the Supporting Information, Figure S4) the height of the granular features was ~60 nm (Table 1). We assume that the granular morphology of the $Au_{9\ nm}$NDT-film with its incomplete coverage resulted from an inhomogeneous structure of the underlying adhesion layer, which provided the template for subsequent deposition of the 9 nm AuNPs. Supporting this assumption, it was reported previously[37] that the layer-by-layer deposition of dodecylamine-stabilized AuNPs typically forms an island structure during the first few deposition cycles.

Electrical Properties and Responses to Tensile Strain. The simple architecture and the dimensions of the resistor

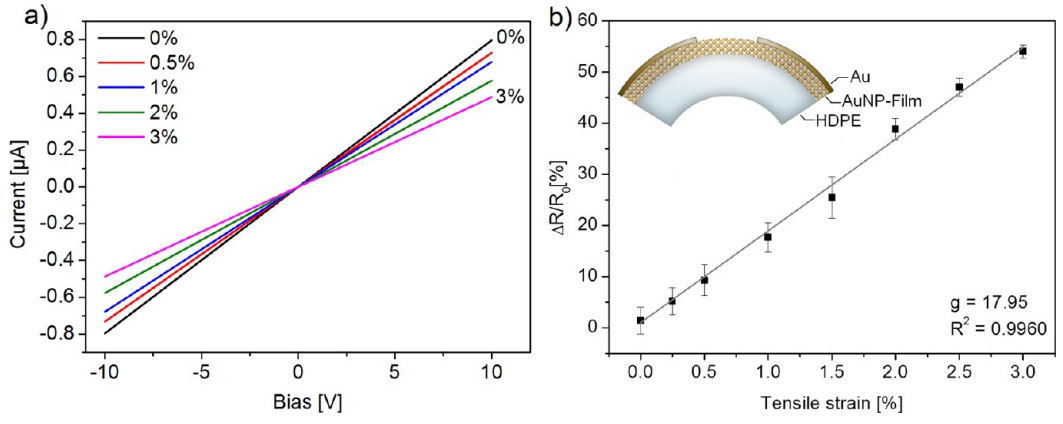

Figure 2. (a) *I*–*V* curves of the film $Au_{4\ nm}$PTM (on HDPE) at initial state and under different strain, as indicated. (b) Relative change in resistance vs tensile strain. The plotted data points were acquired in a set of 4 consecutive strain–relaxation cycles in which the AuNP-film was strained by convex bending of the substrate as shown in the inset. The solid line is a linear fit to the data, with the slope being the gauge factor *g*.

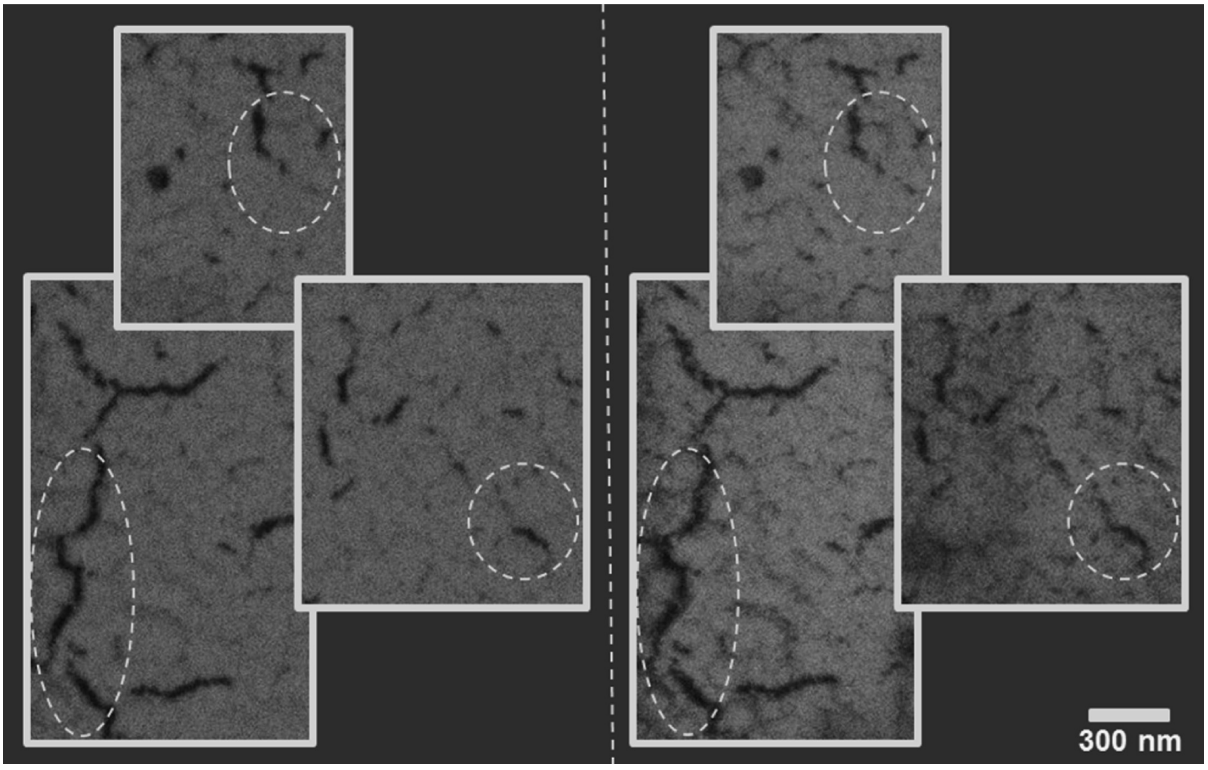

Figure 3. SEM images of the film $Au_{4\ nm}$NDT under no strain (left) and under 3% tensile strain induced in horizontal direction (right). Under strain the cracks are somewhat more pronounced. In order to better recognize the subtle changes of the structure, the images were measured using the backscatter detector to enhance the Z-contrast (see Experimental Section).

devices investigated are depicted in Scheme 1. In the ±10 V range (±250 V cm^{-1}) we observed ohmic current−voltage (I−V) characteristics. Figure 2a shows I−V characteristics of the $Au_{4\ nm}$PTM-film as a representative example.

Table 1 presents the sheet resistances and the estimated conductivities of the three films investigated. The conductivity of the $Au_{4\ nm}$NDT-film is of the same order of magnitude as values reported for the same material deposited on glass[8,38] or LDPE substrates.[11] In contrast, the conductivity of the $Au_{4\ nm}$PTM-film is 1 order of magnitude lower, as can be explained by the larger size of the PTM-linker. In PTM the molecular backbone between the thiol groups is two atoms longer than in NDT. As shown previously, the conductivity of AuNP-films cross-linked with alkanedithiols decreases by approximately 1 order of magnitude when increasing the length of the cross-linker by three methylene units.[38] In addition, the branched structure of PTM, with more than twice the molecular weight of NDT, most likely shields the nanoparticles more efficiently than NDT.

The inhomogeneous morphology makes it difficult to estimate the conductivity of the $Au_{9\ nm}$NDT-film. Assuming an average film thickness of 60 nm with a surface coverage of 75% suggests a conductivity of ~2×10^{-2} $\Omega^{-1}cm^{-1}$. This is approximately three times as large as that of the $Au_{4\ nm}$NDT-film.

The strain sensitivity of the films' conductance was measured by convex bending of the substrates. It should be noted that in this study we investigated the film responses primarily to tensile strain (convex bending), because previous work indicated that compressive strain (concave bending) tends to irreversibly affect the baseline resistance.[11] A set of typical data showing the relative increase in resistance with increasing tensile strain is presented in Figure 2b. These data refer to the film $Au_{4\ nm}$PTM with a gauge factor of ~18. Very similar results were obtained in case of the other two films, $Au_{4\ nm}$NDT and $Au_{9\ nm}$NDT (see the Supporting Information, Figure S5). The gauge factors of all three films are listed in Table 1. These data were measured at ambient conditions. Conducting the experiments under nitrogen resulted in similar gauge factors (see Table 1). Both the linear increase in resistance with tensile strain and the values of the gauge factors are in agreement with data reported for $Au_{4\ nm}$NDT-films on LDPE substrates.[11] Compared to conventional strain gauges based on metal wire grids, the gauge factors reported here are about 1 order of magnitude higher.

Taking into consideration the dominating tunnel term of eq 2, Herrmann et al.[10] proposed the following model to describe the strain gauge response of films made from ligand-stabilized metal nanoparticles

$$\frac{\Delta R}{R_0} = e^{g\varepsilon} - 1 \qquad (3)$$

with $g = \beta(d + \delta_0)$

Here, g is the gauge factor, d is the diameter of the metal cores, δ_0 is the edge-to-edge distance between neighboring metal cores at zero strain, and ε is the strain (i.e., the relative elongation $\Delta l/l_0$ of the film under stress). Contrary to our observation, this model suggests an exponential increase in resistance with increasing strain. Further, using $\beta \approx 10$ nm^{-1} (for alkane chains β values reported range from 9 to 13 nm^{-1})[39] and $\delta_0 \approx 1$ nm[40] the model claims higher gauge factors: ~50 for particles with diameters of 4 nm, and ~100 for particles with diameters of 9 nm.

To explain the differences between our experimental data and eq 3, we need to take into account that the model assumes

a perfectly ordered cubic lattice of particles and, further, that the strain exerted onto the nanoparticle film by geometric expansion of the underlying substrate is translated quantitatively into a uniform increase in interparticle distance. For multilayered, disordered nanoparticle films, it seems more likely that the film responds to strain with structural rearrangements, resulting in a significantly smaller increase in interparticle distance. Recently reported results by Farcau et al.[23] corroborate this assumption. They observed that the gauge factors of monolayered AuNP films were three times larger than those of multilayer films. A smaller effective increase in nanoparticle separation explains not only the low *g*-values observed but also the linear response characteristics, because for an effective strain of only 0.5%, the first order approximation of eq 3 is applicable[10]

$$\frac{\Delta R}{R_0} = g\varepsilon \tag{4}$$

Another factor that should be considered when interpreting the strain gauge responses is the possible strain-induced formation of cracks. Taking into account the heterogeneous nanoscale morphology of the films it seems reasonable to expect that submicrometer cracks and pores are somewhat extended when bending the substrates. Indeed, a comparative SEM investigation of a relaxed $Au_{4\ nm}$NDT-film and of the same film under 3% tensile strain (convex bending) indicated that cracks became somewhat more pronounced under strain, as shown in Figure 3.

The crack hypothesis is further corroborated by another observation: When bending the films for the first few times, we occasionally noticed some minor irreversible increases in resistance, especially when the strain exceeded 1.0%. In that strain range (>1.0%) the $Au_{9\ nm}$NDT-film even showed significant irreversible baseline drifts. Therefore, in the experiments reported here, this particular material was characterized only at lower strain, i.e. $\varepsilon \leq 1.0\%$.

Resistive Responses to Vapors. The resistive responses to vapors were investigated using toluene, 4-methyl-2-pentanone (4M2P), 1-propanol, and water as analytes, with concentrations ranging from 50 to 10 000 ppm. These analytes have similar vapor pressures, but very different polarities.[18] Thus, their partition coefficients for sorption within the films are mainly controlled by their polarity and chemical nature.

In addition to the three films deposited onto HDPE substrates ($Au_{4\ nm}$NDT, $Au_{4\ nm}$PTM, $Au_{9\ nm}$NDT), the chemiresistor responses of a film deposited onto a plasma-treated low density polyethylene (LDPE) substrate were measured, for comparison. This film, which comprises NDT-cross-linked 4 nm sized AuNPs, is referred to as $Au_{4\ nm}$NDT(LDPE).

Figure 4 shows typical responses of the sensors $Au_{4\ nm}$NDT and $Au_{4\ nm}$NDT(LDPE) to toluene vapor.

At a concentration of 500 ppm both sensors displayed fast and reversible response transients. In the case of the film $Au_{4\ nm}$NDT(LDPE), increasing the vapor concentration to 10 000 ppm resulted in a strong signal drift with very slow recovery of the baseline after switching back to carrier gas. In contrast, the film $Au_{4\ nm}$NDT showed only a slight signal drift and fast recovery of the baseline signal. Because it is well-known that LDPE is more permeable to solvent vapors than HDPE,[41] we attribute the slow response/recovery dynamics of the chemiresistor $Au_{4\ nm}$NDT(LDPE) to significant sorption of toluene within the substrate causing the substrate to expand

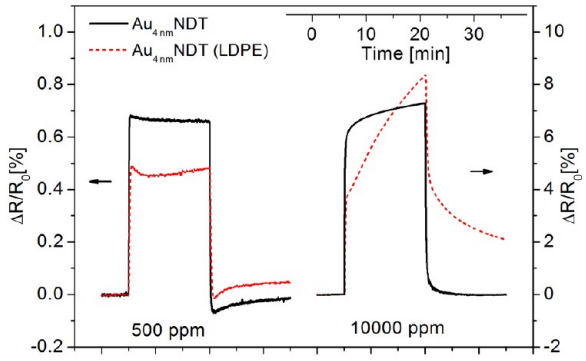

Figure 4. Response transients of AuNP films deposited onto LDPE (dashed red lines) or HDPE (solid black lines) substrates to toluene vapor at concentrations of 500 ppm and 10 000 ppm.

together with the AuNP-coating. Recently, Faupel and coworkers[42] observed similar response/recovery dynamics with chemiresistors based on AuNP-layers, which were deposited onto various polymers via thermal evaporation. They explained the observed baseline drifts by entropy-driven embedding of AuNPs at the polymer surface. Because HDPE is obviously the better suited substrate for chemiresistor applications, all further investigations described herein were carried out with films deposited onto HDPE substrates.

Figure 5a shows the transient responses of the film $Au_{4\ nm}$NDT to the four analytes at various concentrations. The response amplitudes decreased in the order toluene ≈4M2P > 1-propanol > water. The pronounced selectivity for hydrophobic analytes reflects the nonpolar nature of the NDT-linker and is in general agreement with the selectivity of AuNP/alkanedithiol-chemiresistor films deposited onto glass or silicon substrates.[18,38,43] Up to the concentration of 1000 ppm the transients have almost ideal rectangular shapes. For toluene and 4M2P vapors a slow signal rise following the initial steep increase in resistance becomes more and more visible at higher vapor concentrations. In contrast, at high concentrations of 1-propanol a slight decay of the signal intensity following the initial steep increase in resistance is observed. After switching back to carrier gas, transient overshooting is observed, which is more pronounced for the more polar analytes 4M2P and, especially, 1-propanol. In view of the thermally activated tunneling model for charge transport, overshooting can be explained by sorption of analyte within voids in the film, leading to an increased permittivity of the matrix surrounding the AuNPs. This increase in permittivity decreases the activation energy and, thus, decreases the resistance. Taking into consideration the temporal course of the transients, this interpretation implies that after switching from vapor back to carrier gas the initial interparticle distances are restored quickly (reversing film swelling), whereas desorption of analyte from voids happens at a significantly slower rate. A more detailed knowledge about the porous micro- and nanostructure of the film with its impact on the course of sorption processes remains an open key issue for developing a more quantitative understanding of these transient features.

Figure 5b shows the response transients of the chemiresistor $Au_{4\ nm}$PTM. Compared to the $Au_{4\ nm}$NDT-film the selectivity has changed with the response amplitudes decreasing in the order 1-propanol >4M2P ≈ toluene > water (for analyte concentrations >2000 ppm). This change in selectivity is due to the more polar nature of the cross-linker PTM, with its

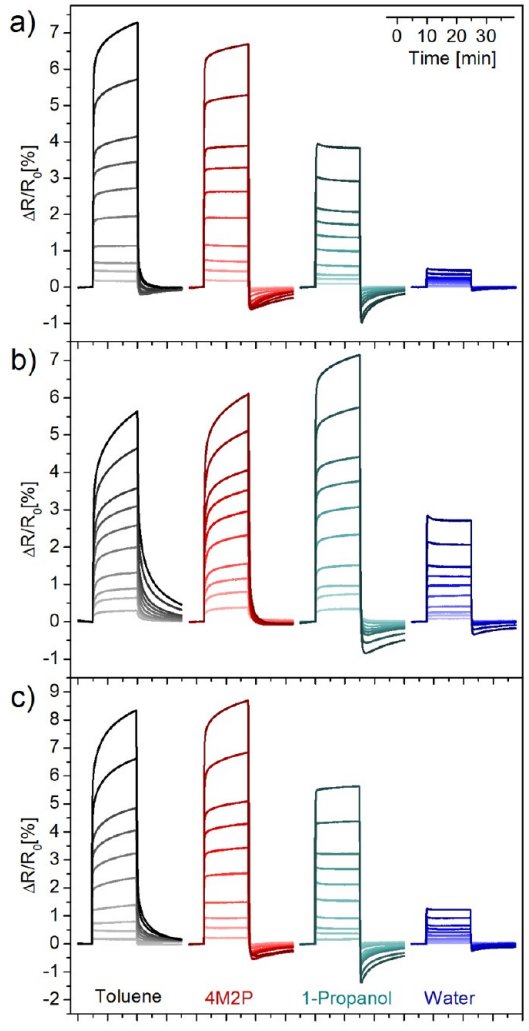

Figure 5. Response transients of (a) $Au_{4\ nm}$NDT, (b) $Au_{4\ nm}$PTM, (c) $Au_{9\ nm}$NDT (all on HDPE) to different solvent vapors. The increase in vapor concentrations (100, 300, 500, 1000, 2000, 3000, 4000, 5000, 7500, 10 000 ppm) is indicated by using light to dark colored graphs.

carbonyl groups providing acceptor sites for the formation of hydrogen bonds with protic polar analytes. Thus, in comparison to the film $Au_{4\ nm}$NDT the response amplitudes measured with 1-propanol and water are significantly enhanced, whereas those measured with the aprotic analytes (4M2P, toluene, at vapor concentrations >4000 ppm) are somewhat suppressed. Overall, the PTM linker has an amphiphilic character due to its polar and nonpolar moieties (ester groups, ethylene groups, neopentylene group). This explains why the responses measured with 1-propanol, 4M2P, and toluene are higher than that of water, despite the polar carbonyl groups of the linker. In comparison to the $Au_{4\ nm}$NDT-film, it is also noticed that the response kinetics for toluene, 4M2P, and 1-propanol vapors are slowed down. We attribute this effect to a higher degree of cross-linking by the tetradentate PTM, enforcing steric hindrance especially of the larger analytes. Overshooting of the transient signals is now observed only in the case of 1-propanol and water vapor. The shape of the transients for water vapor resembles that of the $Au_{4\ nm}$NDT-film for 1-propanol vapor.

Figure 5c shows the transient responses of the chemiresistor $Au_{9\ nm}$NDT. The response amplitudes are somewhat higher, especially for polar analytes, than in case of the $Au_{4\ nm}$NDT film (Figure 5a), but the overall chemical selectivity and the dynamics of the transients are quite similar. This result reveals that the increase in particle size from 4 to 9 nm, as well as the different morphologies of the films (Figure 1), have only a little influence on the selectivity and the response characteristics of the NDT-cross-linked chemiresistor coatings.

At low vapor concentrations (50−500 ppm), the signal transients of all three sensors and for all four analytes showed close to ideal rectangular shapes. The signals' response and recovery times were 10−20 s. Because these values are similar to the time required for exchanging the zero gas by the test gas in the chamber, we conclude that the characteristic t_{90}-times of the sensors were even shorter.

Figure 6a−c shows the response isotherms of the three film materials to all four vapors. In contrast to chemiresistors based on AuNP/alkanedithiol films deposited onto glass or silicon substrates,[38] it was impossible to fit Langmuir isotherms to the data. However, we found good agreement using the Langmuir−Henry sorption model, according to the following equation[17]

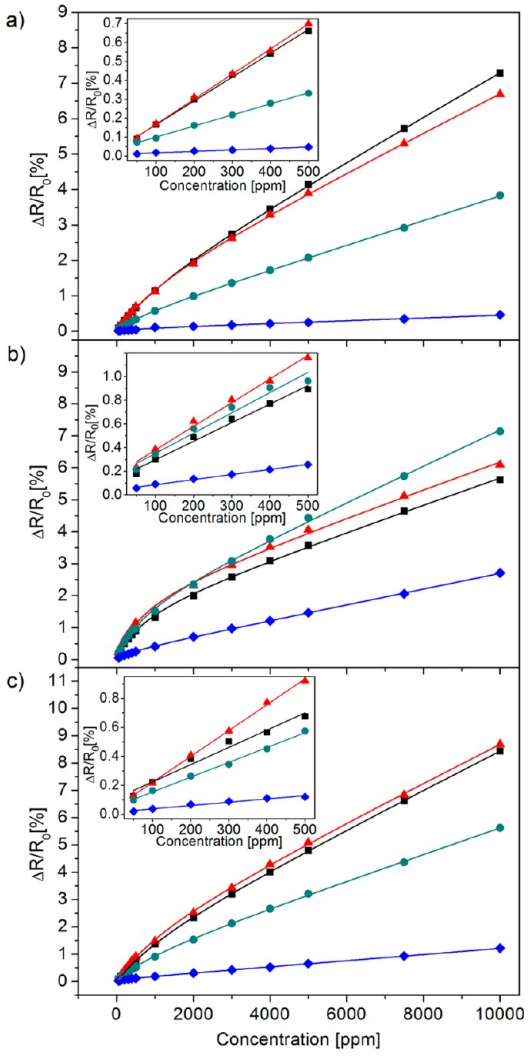

Figure 6. Response isotherms of (a) $Au_{4\ nm}$NDT, (b) $Au_{4\ nm}$PTM, (c) $Au_{9\ nm}$NDT to toluene (black squares), 4M2P (red triangles), 1-propanol (green dots), and water (blue diamonds) fitted with the Langmuir−Henry sorption model (solid lines). The insets show the expanded regions of 50−500 ppm (linear fit).

dx.doi.org/10.1021/am301780b | ACS Appl. Mater. Interfaces 2012, 4, 6151−6161

Table 2. Sensitivities S of the Three Different Films Obtained from Linear Fits of the Response Isotherms in the Concentration Range from 50 to 500 ppm and from 3000 to 10000 ppm (in parentheses)

	S [ppm^{-1}]		
analyte	$Au_{4\ nm}$NDT	$Au_{4\ nm}$PTM	$Au_{9\ nm}$NDT
toluene	$1.26 \times 10^{-5} \pm 3 \times 10^{-7}$	$1.57 \times 10^{-5} \pm 9 \times 10^{-7}$	$1.19 \times 10^{-5} \pm 1.0 \times 10^{-6}$
4M2P	$1.33 \times 10^{-5} \pm 2 \times 10^{-7}$	$2.00 \times 10^{-5} \pm 9 \times 10^{-7}$	$1.78 \times 10^{-5} \pm 3 \times 10^{-7}$
1-propanol	$5.86 \times 10^{-6} \pm 1.0 \times 10^{-7}$($3.51 \times 10^{-6} \pm 3 \times 10^{-8}$)	$1.71 \times 10^{-5} \pm 1.5 \times 10^{-6}$	$1.02 \times 10^{-5} \pm 3 \times 10^{-7}$($4.95 \times 10^{-6} \pm 7 \times 10^{-8}$)
water	$7.65 \times 10^{-7} \pm 3.8 \times 10^{-8}$($4.07 \times 10^{-7} \pm 1.1 \times 10^{-8}$)	$4.29 \times 10^{-6} \pm 1.4 \times 10^{-7}$($2.47 \times 10^{-6} \pm 3 \times 10^{-8}$)	$2.28 \times 10^{-6} \pm 1.9 \times 10^{-7}$($1.13 \times 10^{-6} \pm 1 \times 10^{-8}$)

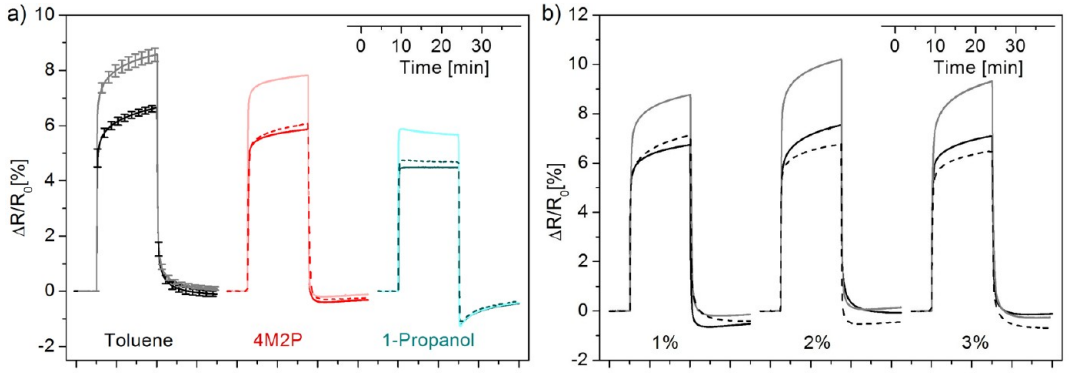

Figure 7. (a) Response transients of the film $Au_{4\ nm}$NDT under no strain (dark solid lines), under 1% strain (light solid lines), remeasured under no strain (dark dashed lines) to different solvent vapors (10 000 ppm). For toluene the error bars shown refer to 5 measurements carried out alternately under strain and under no strain. (b) Response transients of the film $Au_{4\ nm}$NDT to toluene (10 000 ppm) at different strain levels, as indicated.

$$\frac{\Delta R}{R_0} = \left(\frac{\Delta R}{R_0}\right)^{sat} \frac{K_b[A]}{1 + K_b[A]} + K_h[A] \quad (5)$$

The first summand takes into account selective sorption according to the Langmuir model, whereas the second summand takes into account nonselective bulk partitioning according to the Henry model. $((\Delta R)/(R_0))^{sat}$ is the sensor signal when all selective sorption sites in the film are occupied, [A] is the concentration of the vapor, K_b is the Langmuir binding constant, and K_h a constant proportional to Henry's partition coefficient. Langmuir-type sorption at lower analyte concentration and linear Henry-type sorption at higher concentration is known for sorption of gases and vapors in glassy-polymer membranes comprising frozen free-volume voids.[44,45] We note that in order to apply this model to the analysis of chemiresistor responses, it must be assumed that the amplitudes of the signals are directly proportional to the amount of analyte absorbed within the films. In the case of chemiresistors prepared from cross-linked AuNPs this proportionality has been shown experimentally.[17,43]

For all film/vapor pairs, the binding constants K_b of the Langmuir-Henry fits are in the order of $\sim 10^4$ L mol^{-1}. This is 1 order of magnitude higher than previously reported for sorption of toluene in AuNP/alkanedithiol coatings prepared on glass or silicon substrates.[38] We note that in that study the binding constants were extracted using pure Langmuir fits. Tables with all fit parameters are provided as Supporting Information (Table S2).

The sensitivities of the three sensor coatings to different analytes were determined from the slopes of linear curve fits to the response isotherms in the concentration range 50−500 ppm. In this concentration range, all response transients had reached relatively stable values at the end of each vapor dose, i.e., shortly before switching back to carrier gas. The curve fits are shown as insets in Figure 6 and respective sensitivities are listed in Table 2. The sensitivities are similar to those reported by Zhong and co-workers[46] for chemiresistors fabricated from AuNPs on PET substrates. In the case of 1-propanol and water vapors stable response amplitudes were also observed at high vapor concentrations (3000 to 10 000 ppm). For this concentration range, the fit parameter K_h of the Langmuir−Henry model equals the sensitivity. The values are presented in Table 2 in parentheses.

The response isotherms of the two NDT-cross-linked films, $Au_{4\ nm}$NDT and $Au_{9\ nm}$NDT (Figure 5a,c), display qualitatively a very similar appearance in the high concentration range (500−10 000 ppm). This finding confirms a similar chemical selectivity with response amplitudes decreasing in the order toluene ≈4M2P > 1-propanol > water, as already discussed above. However, the sensitivities determined for the low concentration range (50−500 ppm; insets in Figure 6; Table 2) reveal a change in selectivity of the film $Au_{9\ nm}$NDT toward the more polar analytes, with the sensitivities decreasing in the order 4M2P > toluene >1-propanol > water. Further, the sensitivities of the film $Au_{4\ nm}$PTM decrease in the order 4M2P > 1-propanol > toluene > water. Thus, compared to the response amplitudes measured at vapor concentrations above 4000 ppm the order of 4M2P and 1-propanol is reversed.

Responses to Vapors of Films under Tensile Strain. The influence of strain on the chemiresistors' response characteristics was studied by measuring the responses to vapors alternating under tensile strain and under no strain. Figure 7a shows responses of the $Au_{4\ nm}$NDT-film to toluene, 4M2P, and 1-propanol, each at the concentration of 10 000 ppm.

When the sensor was bent to produce 1% strain, the response amplitudes increased by ∼30%. This increase in sensitivity was reversible and highly reproducible, as indicated

by the error bars of the responses to toluene. The transients show that the observed relative increase in response amplitudes was similar for all three vapors. Moreover, similar relative gains of response amplitudes were also observed at lower vapor concentrations, e.g., at 100, 500, and 1000 ppm (see the Supporting Information, Figure S6). In the case of water vapor, the influence of strain on the sensor response was ambiguous and we excluded this analyte from further investigations.

Figure 7b shows the effect of different strain levels on the responses of the $Au_{4\ nm}$NDT-film to toluene vapor (10 000 ppm). At 1% tensile strain the typical ~30% gain of the transient amplitude is seen. Increasing the strain to 2% had a stronger effect with a ~35% relative gain in response amplitude. Further increasing the tensile strain to 3%, however, lowered the strain-induced gain of the response amplitude.

When inducing tensile strain in the films $Au_{4\ nm}$PTM and $Au_{9\ nm}$NDT, we observed a very similar increase in sensitivity, as was seen for the $Au_{4\ nm}$NDT film. Representative data are provided as Supporting Information (Figures S7 and S8). We note that the observed increase in sensitivity caused by bending the films was not affected when varying the current (50−200 nA) used to operate the sensors.

The results reported here are qualitatively in agreement with observations reported by Zhong and co-workers.[26] They investigated strain gauge responses of cross-linked AuNP-films on PET substrates under nitrogen and in various vapor atmospheres. For vapors of analytes, which dissolved well within the film matrix (e.g., hexane, ethanol), the strain gauge responses were significantly stronger than those measured under nitrogen.

In view of the activated tunneling model (eq 2), an enhancement in sensitivity can be caused by two effects. First, if the ability of the sensor film to swell during analyte sorption increases under strain, the perturbation of charge transport via increased tunneling distances becomes more effective. As a consequence the sensitivity increases. Second, if the ability of the film to host guest molecules within voids decreases, the increase in permittivity due to void filling becomes less pronounced. As a consequence, the decrease in activation energy due to analyte sorption becomes weaker, resulting in gain of sensitivity.

To enhance the ability of the sensor films to swell, their freedom to extend in space must be raised. In principle, this can be achieved by loosening the particle network via strain-induced rupture of interconnects and crack formation. Supporting this hypothesis, it has been shown previously that chemiresistors consisting of noninterlinked nanoparticles are more sensitive than those comprising cross-linked nanoparticles.[20] This effect has been assigned to an enhanced ability of the noninterlinked material to swell during analyte sorption. Further, as pointed out above, SEM investigations indicated that cracks became somewhat more pronounced when straining the film $Au_{4\ nm}$NDT by convex bending (Figure 3). Taking into account the reversibility of the strain gauge responses, our interpretation requires that rupture of the particle network and/or crack formation and crack widening are reversible processes.

To enhance the chemical sensitivity by diminishing the permittivity increase during analyte sorption, the accessible void volume must be decreased. In principle, the Poisson effect combined with structural rearrangements may lead to some reduction of void volume when straining the films. However, taking into consideration the expansion of already existing cracks and pores along the strain direction and the formation of new cracks, it seems more likely that tensile strain causes an overall increase in void volume. This net increase in void volume would, contrary to our observation, decrease the sensitivity of the strained sensors.

Taken together, the enhancement in chemical sensitivity caused by inducing tensile strain in the sensors can qualitatively be explained by rupture of the nanoparticle network and formation of cracks, causing an increased ability of the film to swell in lateral direction. The counteracting effect, which is due to the increase in permittivity via sorption of additional analyte in the increased void volume, seems to have only a minor impact.

As mentioned above, compressive strain tends to change the baseline resistance of the films irreversibly. Nevertheless, some experiments were performed to test the influence of compressive strain on the chemiresistors' responses. When inducing 1% compressive strain, the baseline resistance decreased by 14−26%, in reasonable agreement with the gauge factors presented in Table 1. Interestingly, compressive strain enhanced the chemiresistive response amplitudes (see the Supporting Information, Figure S9), but the effect was less pronounced than for films under tensile stress. According to our discussion above, the enhancement in sensitivity of films under compressive stress suggests that compression reduces the accessible void volume, and thus, diminishes the permittivity increase during vapor sorption. At the same time, the ability of film swelling in the direction normal to the film surface remains rather unaffected because concave bending compresses the film only in lateral direction. Taking into account the inhomogeneous nanoscale morphology of the films, it also appears plausible that compressive stress induces structural dislocations and rearrangements involving rupture of interparticle linkages. This, again, would increase the ability of the film to swell, and thus, would enhance the chemiresistive sensitivity.

SUMMARY AND CONCLUSIONS

In this study, we deposited cross-linked AuNPs onto plasma-treated HDPE substrates via layer-by-layer self-assembly. Testing the films as strain gauges revealed gauge factors of ~20 ($Au_{4\ nm}$NDT, $Au_{4\ nm}$PTM) and ~25 ($Au_{9\ nm}$NDT). These values are lower than suggested by the tunneling model for charge transport. To explain this difference we propose that the films are not strained evenly when bending the substrates. More likely, structural reorganization, reversible extension of existing cracks and the formation of new cracks on the nanometer scale have to be taken into account for better understanding the strain sensing mechanism.

An AuNP-film deposited onto LDPE showed very slow chemiresistor responses when dosed with concentrated toluene vapor. We assign this effect to significant sorption of toluene within the substrate. Much faster responses were obtained for AuNP-films on HDPE substrates, which are more resistant to organic solvents. The chemical sensitivity of the film $Au_{4\ nm}$NDT decreased with the polarity of the analytes: toluene ≈4M2P > 1-propanol > water. Films comprising differently sized AuNPs (4 and 9 nm core diameter) showed similar chemical selectivity and sensitivities, especially at higher vapor concentrations (>4000 ppm). Using the more polar PTM as cross-linker selectively enhanced the sensitivities to 1-propanol and water. The response isotherms of all three films for vapors in the concentration range from 50 to 10 000 ppm were well reproduced using a Langmuir−Henry sorption model.

In general, the chemiresistor response transients were characterized by a net increase in resistance, suggesting that swelling is the dominant component of the sensing mechanism. For the more polar analytes, however, pronounced negative overshooting of the transients was observed after switching back from vapor atmosphere to carrier gas. In view of the activated tunneling model, this signature was assigned to slow desorption of the analyte from voids.

By inducing 1% tensile strain, the sensitivity of the chemiresistors was enhanced by ∼30%, regardless of the analyte's polarity. We assigned this enhancement to reversible rupture of the particle network and crack formation increasing the freedom of the films to swell in lateral direction during analyte sorption. This explanation is supported by comparative SEM measurements of the $Au_{4\ nm}$NDT-film in the relaxed state and under 3% tensile strain. Further, compressive strain also enhanced the chemiresistive response amplitudes, but the effect was less pronounced than in the case of films under tensile strain. Tentatively, we attributed this effect to a decreased void volume of the compressed film.

To study strain-induced structural changes in AuNP-films in more detail and to understand more quantitatively their impact on the conductivity and chemiresistive responses, we are currently focusing our research efforts on the preparation and characterization of highly ordered nanoparticle films. Structural changes in these materials can be studied with high resolution by various in situ scattering methods. For example, Siffalovic et al.[47] demonstrated that in situ small-angle X-ray scattering (SAXS) is well-suited to investigating the increase in spacing of non-cross-linked iron oxide nanoparticles when applying tensile strain to the underlying substrate.

■ ASSOCIATED CONTENT

Supporting Information

TEM images of the gold nanoparticles, SEM images and photographs of the gold nanoparticle films, IR spectra of the HDPE substrate before and after plasma treatment, resistive responses to tensile strain, response transients of the films under strain to different vapors and with varying concentration, Langmuir−Henry fit parameters. This material is available free of charge via the Internet at http://pubs.acs.org.

■ AUTHOR INFORMATION

Corresponding Author

*E-mail: tobias.vossmeyer@chemie.uni-hamburg.de.

Present Address

† Institute of Technical and Macromolecular Chemistry, University of Hamburg, Bundesstraße 45, 20146 Hamburg, Germany

Author Contributions

The manuscript was written through contributions of all authors. All authors have given approval to the final version of the manuscript.

Notes

The authors declare no competing financial interest.

■ ACKNOWLEDGMENTS

The authors thank Mr. Jan H. Schröder and Mr. Sedat Dogan for technical assistance regarding the vapor deposition of gold electrodes. Mr. Andreas Kornowski is acknowledged for measuring the SEM images shown in Figures 1 and 3 and in the Supporting Information. We thank Mr. Mateusz Olichwer for supporting the preparation of graphical artwork. Mr. Adam Steiger is acknowledged for proofreading major parts of the manuscript.

■ REFERENCES

(1) Terrill, R. H.; Postlethwaite, T. A.; Chen, C.-H.; Poon, C.-D.; Terzis, A.; Chen, A.; Hutchison, J. E.; Clark, M. R.; Wignall, G.; Londono, J. D.; Superfine, R.; Falvo, M.; Johnson, C. S., Jr.; Samulski, E. T.; Murray, R. W. *J. Am. Chem. Soc.* **1995**, *117*, 12537−12548.

(2) Wuelfing, W. P.; Green, S. J.; Pietron, J. J.; Cliffel, D. E.; Murray, R. W. *J. Am. Chem. Soc.* **2000**, *122*, 11465−11472.

(3) Wohltjen, H.; Snow, A. S. *Anal. Chem.* **1998**, *70*, 2856−2859.

(4) Evans, S. D.; Johnson, S. R.; Cheng, Y. L.; Shen, T. *J. Mater. Chem.* **2000**, *10*, 183−188.

(5) Han, L.; Daniel, D. R.; Maye, M. M.; Zhong, C.-J. *Anal. Chem.* **2001**, *73*, 4441−4449.

(6) Zamborini, F. P.; Leopold, M. C.; Hicks, J. F.; Kulesza, P. J.; Malik, M. A.; Murray, R. W. *J. Am. Chem. Soc.* **2002**, *124*, 8958−8964.

(7) Vossmeyer, T.; Guse, B.; Besnard, I.; Bauer, R. E.; Müllen, K.; Yasuda, A. *Adv. Mater.* **2002**, *14*, 238−242.

(8) Joseph, Y.; Besnard, I.; Rosenberger, M.; Guse, B.; Nothofer, H.-G.; Wessels, J. M.; Wild, U.; Knop-Gericke, A.; Su, D.; Schlögl, R.; Yasuda, A.; Vossmeyer, T. *J. Phys. Chem. B* **2003**, *107*, 7406−7413.

(9) Steinecker, W. H.; Rowe, M. P.; Zellers, E. T. *Anal. Chem.* **2007**, *79*, 4977−4986.

(10) Herrmann, J.; Müller, K.-H.; Reda, T.; Baxter, G. R.; Raguse, B.; de Groot, G. J. J. B.; Chai, R.; Roberts, M.; Wieczorek., L. *Appl. Phys. Lett.* **2007**, *91*, 183105(3pp).

(11) Vossmeyer, T.; Stolte, C.; Ijeh, M.; Kornowski, A.; Weller, H. *Adv. Funct. Mater.* **2008**, *18*, 1611−1616.

(12) Briglin, S. M.; Gao, T.; Lewis, N. S. *Langmuir* **2004**, *20*, 299−305.

(13) Peng, G.; Tisch, U.; Adams, O.; Hakim, M.; Shehada, N.; Broza, Y. Y.; Billan, S.; Abdah-Bortnyak, R.; Kuten, A.; Haick, H. *Nat. Nanotechnol.* **2009**, *4*, 669−673.

(14) Zhong, Q.; Steinecker, W. H.; Zellers, E. T. *Analyst* **2009**, *134*, 283−293.

(15) García-Berríos, E.; Gao, T.; Theriot, J. C.; Woodka, M. D.; Brunschwig, B. S.; Lewis, N. S. *J. Phys. Chem. C* **2011**, *115*, 6208−6217.

(16) Im, J.; Sengupta, S. K.; Baruch, M. F.; Granz, C. D.; Ammu, S.; Manohar, S. K.; Whitten, J. E. *Sens. Actuators, B* **2011**, *156*, 715−722.

(17) Krasteva, N.; Fogel, Y.; Bauer, R. E.; Müllen, K.; Joseph, Y.; Matsuzawa, N.; Yasuda, A.; Vossmeyer, T. *Adv. Funct. Mater.* **2007**, *17*, 881−888.

(18) Joseph, Y.; Peić, A.; Chen, X.; Michl, J.; Vossmeyer, T.; Yasuda, A. *J. Phys. Chem. C* **2007**, *111*, 12855−12859.

(19) Zhang, H.-L.; Evans, S. D.; Henderson, J. R.; Miles, R. E.; Shen, T.-H. *Nanotechnology* **2002**, *13*, 439−444.

(20) Ibañez, F. J.; Gowrishetty, U.; Crain, M. M.; Walsh, K. M.; Zamborini, F. P. *Anal. Chem.* **2006**, *78*, 753−761.

(21) García-Berríos, E.; Gao, T.; Woodka, M. D.; Maldonado, S.; Brunschwig, B. S.; Ellsworth, M. W.; Lewis, N. S. *J. Phys. Chem. C* **2010**, *114*, 21914−21920.

(22) Ibañez, F. J.; Zamborini, F. P. *Small* **2011**, *8*, 174−202.

(23) Farcau, C.; Moreira, H.; Viallet, B.; Grisolia, J.; Ciuculescu-Pradines, D.; Amiens, C.; Ressier, L. *J. Phys. Chem. C* **2011**, *115*, 14494−14499.

(24) Farcau, C.; Sangeetha, N. M.; Moreira, H.; Viallet, B.; Grisolia, J.; Ciuculescu-Pradines, D.; Ressier, L. *ACS Nano* **2011**, *5*, 7137−7143.

(25) Radha, B.; Sagade, A. A.; Kulkarni, G. U. *ACS Appl. Mater. Interfaces* **2011**, *3*, 2173−2178.

(26) Yin, J.; Hu, P.; Luo, J.; Wang, L.; Cohen, M. F.; Zhong, C.-J. *ACS Nano* **2011**, *8*, 6516−6526.

(27) Leff, D. V.; Brandt, L.; Heath, J. R. *Langmuir* **1996**, *12*, 4723−4730.

(28) Shen, C.; Hui, C.; Yang, T.; Xiao, C.; Tian, J.; Bao, L.; Chen, S.; Ding, H.; Gao, H. *Chem. Mater.* **2008**, *20*, 6939−6944.

(29) Bethell, D.; Brust, M.; Schiffrin, D. J.; Kiely, C. *J. Electroanal. Chem.* **1996**, *409*, 137−143.
(30) Schlicke, H.; Schröder, J. H.; Trebbin, M.; Petrov, A.; Ijeh, M.; Weller, H.; Vossmeyer, T. *Nanotechnology* **2011**, *22*, 305303(9pp).
(31) Clouet, F.; Shi, M. K. *J. Appl. Polym. Sci.* **1992**, *46*, 1955−1966.
(32) Shikova, T. G.; Rybkin, V. V.; Titov, V. A.; Choi, H.-S. *High Energy Chem.* **2006**, *40*, 351−355.
(33) Greene, G.; Yao, G.; Tannenbaum, R. *Langmuir* **2003**, *19*, 5869−5874.
(34) Choi, D. M.; Park, C. K.; Cho, K.; Park, C. E. *Polymer* **1997**, *38*, 6243−6249.
(35) Llop, C.; Manrique, A.; Navarro, R.; Mijangos, C.; Reinecke, H. *Polym. Eng. Sci.* **2011**, *51*, 1763−1769.
(36) Lin, Y.; Skaff, H.; Böker, A.; Dinsmore, A. D.; Emrick, T.; Russell, T. P. *J. Am. Chem. Soc.* **2003**, *125*, 12690−12691.
(37) Joseph, Y.; Guse, B.; Vossmeyer, T.; Yasuda, A. *J. Phys. Chem. C* **2008**, *112*, 12507−12514.
(38) Vossmeyer, T.; Joseph, Y.; Besnard, I.; Harnack, O.; Krasteva, N.; Guse, B.; Nothofer, H.-G.; Yasuda, A. *SPIE* **2004**, *5513*, 202−212.
(39) Adams, D. M.; Brus, L.; Chidsey, C. E. D.; Creager, S.; Creutz, C.; Kagan, C. R.; Kamat, P. V.; Liebermann, M.; Lindsay, S.; Marcus, R. A.; Metzger, R. M.; Michel-Beyerle, M. E.; Miller, J. R.; Newton, M. D.; Rolison, D. R.; Sankey, O.; Schanze, K. S.; Yardley, J.; Zhu, X. *J. Phys. Chem. B* **2003**, *107*, 6668−6697.
(40) The length of the all-trans alkylene chain in 1,9-nonanedithiol is 1.13 nm, using 1.25A° per methylene unit.
(41) Carlowitz, B. *Kunststoff-Tabellen, 4., völlig überarbeitete und erweiterte Auflage*; Carl Hanser Verlag: München, Germany, 1995.
(42) Hanisch, C.; Kulkarni, A.; Zaporojtchenko, V.; Faupel, F. *J. Phys.: Conf. Ser.* **2008**, *100*, 052043(4pp).
(43) Joseph, Y.; Krasteva, N.; Besnard, I.; Guse, B.; Rosenberger, M.; Wild, U.; Knop-Gericke, A.; Schlögl, R.; Krustev, R.; Yasuda, A.; Vossmeyer, T. *Faraday Discuss.* **2004**, *125*, 77−97.
(44) Klopffer, M. H.; Flaconnèche, B. *Oil Gas Sci. Technol.* **2001**, *56*, 223−244.
(45) Tsujita, Y. *Prog. Polym. Sci.* **2003**, *28*, 1377−1401.
(46) Wang, L.; Luo, J.; Yin, J.; Zhang, H.; Wu, J.; Shi, X.; Crew, E.; Xu, Z.; Rendeng, Q.; Lu, S.; Poliks, M.; Sammakia, B.; Zhong, C.-J. *J. Mater. Chem.* **2010**, *20*, 907−915.
(47) Siffalovic, P.; Chitu, L.; Vegso, K.; Majkova, E.; Jergel, M.; Weis, M.; Luby, S; Capek, I.; Keckes, J.; Maier, G. A.; Satka, A.; Perlich, J.; Roth, S. V. *Nanotechnology* **2010**, *21*, 385702(5pp).